JGR Biogeosciences

RESEARCH ARTICLE
10.1029/2019JG005172

Tall Tower Ammonia Observations and Emission Estimates in the U.S. Midwest

Timothy J. Griffis[1], Cheng Hu[1], John M. Baker[1,2], Jeffrey D. Wood[3], Dylan B. Millet[1], Mathew Erickson[1], Zhongjie Yu[1], M. Julian Deventer[1], Cody Winker[2], and Zichong Chen[1]

[1]Department of Soil, Water, and Climate, University of Minnesota, St. Paul, MN, USA, [2]United States Department of Agriculture, Agricultural Research Service, St. Paul, MN, USA, [3]School of Natural Resources, University of Missouri, Columbia, MO, USA

Key Points:
- Observations of NH3 from a tall tower (100 m) provide insights regarding regional emissions from the US Corn Belt
- Annual NH3 emissions estimated using state-of-the-art inventories were 0.6 to 1.4-fold compared to the tall tower flux density
- Annual gross emission estimates for the Upper Midwest and broader US Corn Belt regions were +720 Gg NH3-N y^{-1} and +1340 Gg NH3-N y^{-1}

Supporting Information:
- Supporting Information S1

Correspondence to:
T. J. Griffis,
timgriffis@umn.edu

Citation:
Griffis, T. J., Hu, C., Baker, J. M., Wood, J. D., Millet, D. B., Erickson, M., et al (2019). Tall tower ammonia observations in the U.S. Midwest. *Journal of Geophysical Research: Biogeosciences*, *124*, 3432–3447. https://doi.org/10.1029/2019JG005172

Received 30 MAR 2019
Accepted 20 SEP 2019
Accepted article online 10 OCT 2019
Published online 16 NOV 2019

©2019. American Geophysical Union. All Rights Reserved.

Abstract Atmospheric ammonia (NH_3) has increased dramatically as a consequence of the production of synthetic nitrogen (N) fertilizer and proliferation of intensive livestock systems. It is a chemical of environmental concern as it readily reacts with atmospheric acids to produce fine particulate matter and indirectly contributes to nitrous oxide (N_2O) emissions. Here, we present the first tall tower observations of NH_3 within the U.S. Corn Belt for the period April 2017 through December 2018. Hourly average NH_3 mixing ratios were measured at 100 and 56 m above the ground surface and fluxes were estimated using a modified gradient approach. The highest NH_3 mixing ratios (>30 nmol mol^{-1}) occurred during early spring and late fall, coinciding with the timing of fertilizer application within the region and the occurrence of warm air temperatures. Net ecosystem NH_3 exchange was greatest in spring and fall with peak emissions of about +50 nmol m^{-2} s^{-1}. Annual NH_3 emissions estimated using state-of-the-art inventories ranged from 0.6 to 1.4 × the mean annual gross tall tower fluxes (+2.1 nmol m^{-2} s^{-1}). If the tall tower observations are representative of the Upper Midwest and broader U.S. Corn Belt regions, the annual gross emissions were +720 Gg NH_3-N y^{-1} and +1,340 Gg NH_3-N y^{-1}, respectively. Finally, considering the N_2O budget over the same region, we estimated total reactive N emissions (i.e., N_2O + NH_3) of approximately 1,790 Gg N y^{-1} from the U.S. Corn Belt, representing ~23% of the current annual new N input.

1. Introduction

Agricultural systems are having a profound influence on the global nitrogen (N) cycle and the flux of reactive nitrogen (N_r) between the biosphere and atmosphere (Erisman et al., 2008; Sutton et al., 2013; Zhang et al., 2015). The massive increase in synthetic N fertilizer has caused global emissions of ammonia (NH_3) to increase nearly 500% during the 20th century (Bouwman et al., 2013) and that trend is expected to accelerate through the 21st century (Ciais et al., 2013). Ammonia is a chemical of significant environmental concern as it readily reacts with atmospheric acids to produce fine particulate matter ($PM_{2.5}$); it is thus linked to human health impacts with agricultural emissions costing the United States approximately $36 billion (2006 USD) annually (Paulot & Jacob, 2014). Ammonia also has deleterious effects on natural terrestrial and aquatic ecosystems (Britto & Kronzucker, 2002; Fangmeier et al., 1994; Sheppard et al., 2011). Furthermore, NH_3 deposition can also indirectly enhance nitrous oxide (N_2O) emissions (Pinder et al., 2013). The development of regulations to reduce $PM_{2.5}$ and NH_3 emissions in the United States is under consideration and will require improved understanding of NH_3 sources, sinks, and transport processes (Felix et al., 2017; Schwede et al., 2016).

Knowledge regarding the NH_3 budget of the U.S. Midwest and Corn Belt has lagged behind that for N_2O. Based on satellite observations, the U.S. Midwest has been identified as a global hotspot for NH_3 emissions (Paulot et al., 2014; Shephard et al., 2011; Van Damme et al., 2014, 2015). The estimated source strength is on the order of 500 Gg NH_3-N y^{-1} and is comparable in magnitude to the N_2O-N budget for the region (Chen et al., 2016; Griffis et al., 2013, 2017; Van Damme et al., 2014). However, we are unaware of any systematic tall tower-based systems that have been used to measure fluxes to help verify such estimates.

The mosaic of crops, natural ecosystems, and high density of dairy, beef, swine, and poultry operations within the Corn Belt is likely to produce high spatial and temporal heterogeneity of NH_3 sinks and sources. Point source emissions of NH_3 from livestock farms are subject to significant dry deposition within tens of

kilometer from the source, which can later be volatilized (Asman et al., 1998; Loubet et al., 2006; Vogt et al., 2013; Walker et al., 2014). Given such spatiotemporal heterogeneity in the NH_3 bidirectional exchange, bottom-up budgets remain highly uncertain (Bash et al., 2013; Schlesinger, 2009; Sutton et al., 2013), and tall tower top-down approaches could provide a powerful constraint on these emission estimates. Indeed, a recent 28-day campaign from the Boulder Atmospheric Observatory tall tower (Colorado, USA) has provided novel insights regarding the large dynamic range of atmospheric NH_3 mixing ratios (i.e., below detection limit to 192 nmol mol^{-1}) and positive and negative vertical gradients indicating both NH_3 net sink and source behavior depending on air mass and environmental characteristics (Tevlin et al., 2017).

The objectives of this paper, therefore, were to obtain insights regarding the regional (i.e,. within the U.S. Corn Belt) behavior of NH_3 mixing ratios and fluxes and to constrain the annual budget based on high temporal resolution tall tower observations. Here, we address these objectives using mean hourly observations collected from a tall tower in southern Minnesota over the period April 2017 to December 2018.

2. Methods

2.1. Study Site

The University of Minnesota tall tower trace gas observatory is located about 25-km south of the Saint Paul—Minneapolis Metropolitan area in the Upper Midwest, United States (KCMP radio tower, 44° 41′ 19″ N, 93° 40′ 22″ W; 290 m ASL). The landscape is highly heterogeneous with agricultural lands predominant to the east, south, and west. Detailed land use statistics, as a function of distance and direction from the tall tower site, have been reported previously (Griffis et al., 2013; Zhang et al., 2014). Land use characteristics for wind and air masses originating from 30 to 290 degrees are dominated by corn (28%), soybean (18%), grassland (23%), woodlands (12%), wetlands (10%), and open water (6%; Griffis et al., 2010). These land use statistics are typical of the Corn Belt (Zhang et al., 2014). Further, there are a number of major livestock facilities located within 50 km of the tall tower, with total cattle, hog, and poultry populations of approximately 190,000, 232,000, and 434,000, respectively (Minnesota Pollution Control Agency, 2015).

2.2. Ammonia Mixing Ratio Observations

The KCMP tall tower has been instrumented with meteorological and trace gas sensors since April 2007. Carbon dioxide, water vapor, nitrous oxide, and methane have been measured at sample heights of 32, 56, 100, and 185 m (Griffis et al., 2013; Griffis et al., 2016; Zhang et al., 2014). Turbulence is measured at 100 and 185 m using sonic-anemometers (model CSAT3; Campbell Scientific Inc. Logan, Utah). Near-continuous measurement of NH_3 mixing ratios was initiated in March 2017 using an off-axis cavity ring-down spectrometer (EAA-30-EP, Los Gatos Research [LGR], San Jose, CA, USA) with an enhanced thermal stability option to reduce measurement drift. The manufacturer's reported measurement NH_3 noise (1 σ) is <0.2 nmol mol^{-1} for an integration period of 100 s. Based on our own calibrations, using a custom NH_3 permeation device at the field site, we calculated an Allan deviation of 0.24 nmol mol^{-1} for an integration period of 100 s (supporting information, Figure S1). Note that some thermal instability in the calibration device can contribute to this instrument noise estimate. Based on sampling from a large (240 L) buffer volume, with near constant NH_3 mixing ratio, the LGR measurement noise reached a minimum of <0.19 nmol mol^{-1} for an integration period of about 600 s and remained relatively low (< 0.26 nmol mol^{-1}) for an integration period exceeding 1 hr (Figure S2). Our automated calibration strategy was performed to check the zero each hour and the span once per week. This analyzer also measures water vapor mixing ratio, which was used here as a performance diagnostic and was compared with simultaneous measurements from an infrared gas analyzer (LI-7000, Li-Cor Inc., Lincoln, NB, USA) system (Figure S3).

Through laboratory testing of the NH_3 analyzer we observed spectral interference between the water vapor and NH_3 channels, where an increase in water vapor mixing ratio caused an increase in the recorded NH_3 mixing ratio. This type of spectral interference has been observed in similar analyzers used to measure NH_3 and stable isotopes of carbon dioxide (Martin et al., 2016; Xu et al., 2017). Here, we characterized and corrected for this water vapor dependence based on a series of calibration tests with varying water vapor

mixing ratios. Specifically, we supplied a mixing ratio generator (Baker & Griffis, 2010) with ultra-zero dry air and slowly increased the water vapor mixing ratio. The NH_3 analyzer sampled this air stream continuously at 1.5 SLPM. Figure S4 illustrates the influence of water vapor on the NH_3 measurement. Based on linear regression, the sensitivity of NH_3 to water vapor was approximately 0.41 ± 0.11 nmol mol^{-1} per mmol mol^{-1} of water vapor ($r^2 = 0.75$, $p = 0.007$). We have corrected the tall tower NH_3 measurements according to this sensitivity. The water vapor interference correction had a small influence on the absolute mixing ratios measured at both tall tower sample levels, and therefore, very little influence on the flux-gradient estimates described below.

To facilitate the tall tower NH_3 sampling we installed new Teflon sample lines (TPH0308-063 PFA 3/8 "ID × 1/2"OD, Jensen Inert Products, Coral Springs, FL, USA) at 100 and 56 m above the ground on 21 March 2017. The two sample lines had an identical total length of 130 m in order to maintain consistent flow rate and sample air pressure in both lines and to minimize the potential for differential effects of tubing wall interactions (adsorption/desorption) on NH_3. A similar strategy using long (100 m) polyethylene sample lines was used to measure NH_3 fluxes over multiple agricultural plots (Warland et al., 2001). Teflon filter holders (12,009-4 m-147-4 m PFA filter 47 mm × 1/4"MNPT × 1/4" MNPT tefzel clamp, Jensen Inert Products) were installed at the inlets on the tower and before the subsample manifold located upstream of the NH_3 analyzer. Sample lines were insulated with dense foam and heated using heat tape (Chromalox SRL, UT, USA) from the base of the tower to the manifold that was housed in a climate controlled building to prevent condensation. Further, a second set of Teflon lines were installed that permit injection of gas standards from the base of the tall tower to the 56- and 100-m sample inlets using Teflon tee connectors. This was designed for diagnostic testing of the sampling system and analyzer and to periodically estimate the flux noise (flux detection limit) of the system. Air was pulled continuously down the sample lines at a flow rate of 8 SLPM and subsampled by the LGR analyzer at 1.5 SLPM. The sampling sequence consisted of 1) sampling of the 100-m level for 120 s; 2) sampling the 56-m level for 120 s); 3) sampling ultra-pure dry air once per hour; and 4) span calibration once per week using a thermostatically controlled permeation device. The custom built calibration device consisted of a thermostatically controlled Teflon block with a channel fitted with an NH_3 permeation tube (Ammonia Wafer Device Type 60F3, VICI Metronics, Poulsbo, Washington, USA with total permeation rate of 25 ng per min, certified rate at 35 °C is ±2 ng) connected to a water vapor mixing ratio generator (Baker & Griffis, 2010).

Lagged covariance time series analyses were performed to examine if there were any significant lag effects associated with the adsorption and desorption of NH_3 to the Teflon sample lines. These analyses showed a pronounced peak in covariance observed at a sample lag of 0 hr for NH_3 measured at the 100- and 56-m levels. Further, there was a well-defined peak with maximum covariance at a sample lag of 0 hr among NH_3 and water vapor and NH_3 and sonic-derived air temperature, respectively (Figures S5 and S6). Similar analyses conducted at shorter timescales (seconds to minutes) also showed that lag effects were small compared to the hourly averaging periods used for flux calculations. Further, the transient response of the tall tower subsampling system and the 100-m sample inlet are shown in Figures S7–S9 demonstrating that tubing interactions did not significantly limit the dynamic performance of the system for measuring changes in NH_3 mixing ratios.

We selected four of the closest active sites from the Ammonia Monitoring Network (AMoN, http://nadp.slh.wisc.edu/amon/) for qualitative comparison of NH_3 mixing ratio variability with the tall tower observations (Figure S10). These sites included Wisconsin (WI35 and WI07), Nebraska (NE98), and Illinois (IL37). The AMoN network uses chemical samplers (Radiello, Sigma-Aldrich, MO, USA) mounted 2 m above the ground surface and sheltered from precipitation. Ammonia in ambient air is absorbed continually by the interior surface of the sampler and converted to NH_4^+. The sample integration period represents 2 weeks (Schrader et al., 2018).

2.3. Ammonia Flux Estimates

The hourly net ecosystem NH_3 exchange (NEE) was estimated using a modified Bowen-ratio approach (Hicks & Wesely, 1978; Walker et al., 2006). First, the eddy covariance technique was used to estimate the water vapor and carbon dioxide fluxes measured at the tall tower (Griffis et al., 2010; Wood et al., 2017;

Zhang et al., 2014). The eddy diffusivity for water vapor (K_w) and carbon dioxide (K_c) was estimated from the inversion of the eddy flux and tall tower scalar gradients as:

$$K_w = \frac{F_C}{M_a \frac{dC}{dz}} \quad (1)$$

where F_C is the eddy flux of water vapor or carbon dioxide, dC/dz is the corresponding scalar concentration gradient, and M_a is the molar air density. Here, we are making two assumptions: First, the measurements are taken from within the constant flux layer, which is a reasonable assumption for heights above the roughness sublayer and below about 200 m (Griffis et al., 2010); Second, there is similarity between the eddy diffusivity of NH_3 (K_A) and K_w. A similar approach has used the sensible heat flux to derive K_A (Bash et al., 2010; Walker et al., 2006). For cases when K_w was physically unrealistic or missing we applied K_C. For cases when K_w and K_C were both invalid or missing we calculated the eddy diffusivity based on the momentum flux derived from eddy covariance observations with stability corrections applied. Finally, the ammonia NEE was calculated as the sum of the turbulent flux and the change in hourly storage measured below the 100-m level,

$$\mathrm{NEE} = -M_a K_A \frac{dC}{dz} + M_a \int \frac{dC}{dt} dz. \quad (2)$$

Over the course of the growing season (April through August), the diel range of variation for the median storage flux and turbulent flux varied from −0.07 to 0.1 nmol m^{-2} s^{-1} and 0.05 to 0.5 nmol m^{-2} s^{-1}, respectively.

2.4. Quality Control of NH_3 Mixing Ratios and Fluxes

Ammonia mixing ratios were filtered for periods when the NH_3 analyzer measured anomalous (i.e., 10 mmol mol^{-1}) water vapor mixing ratios based on comparison with the infrared gas analyzer (LI7000). Further, we filtered out NH_3 observations obtained during strongly condensing conditions. These periods were identified when the water vapor mixing ratio differences between the 100- and 56-m levels were more negative than −0.5 mmol mol^{-1} (i.e., when the water vapor gradient was strong and directed toward the land surface). Finally, we filtered out NH_3 fluxes when the atmosphere was strongly stable (i.e., when [z-d]/L exceeded a value of +4.5) and subject to decoupling from the surface fluxes. Approximately 35.1% of the hourly flux data were either missing due to instrument failure or filtered according to the above quality control procedures.

The minimum detectable NH_3 flux was estimated from a zero flux-gradient test in situ by injecting standard dry air to both the 56- and 100-m levels over a period of 3 days. These data were then processed using the flux-gradient calculations described above to estimate the flux noise. Note that in this case the eddy diffusivity was calculated from the momentum flux because the gradients of water vapor and carbon dioxide were altered by the dry air injection. This test is analogous to conducting a blank chamber measurement or characterizing flux noise in eddy covariance measurements when the air sample is provided by a stable gas cylinder (Griffis et al., 2008). Here, the flux noise (mean ± SE) was estimated to be 0.005 ± 0.007 nmol m^{-2} s^{-1} (Figure S11). Overall, about 69% of the remaining flux-gradient observations were greater than the detection limit.

2.5. Wet Deposition of Nitrogen

Precipitation samples were collected using an automated NADP-approved system (model MDN 00–125-4; N-CON Systems Co., Inc.; Crawford, GA, USA) to measure wet deposition of nutrients and acidity. The sampler was equipped for thermostatic storage (model 17–126, N-CON Systems Co., Inc.), with samples collected into acid-rinsed glass flasks to optimize preservation (Krupa, 2002). Samples were collected weekly, were kept frozen prior to analysis, and were subsampled and analyzed using a Lachat Flow Injection Analyzer (Lachat Instruments, Milwaukee, WI, USA) to quantify NO_3-N and NH_3-N concentrations. Precipitation amounts were measured using an all-weather precipitation weighing gauge (Geonor Inc., Augusta, NJ, USA) located near the deposition sampler. Precipitation amounts and nitrogen (N) concentrations were used to calculate wet N deposition on a mass per unit area basis.

2.6. Nitrogen Use and Ammonia Sources From Emission Inventories

Fertilizer and manure surveys conducted for Minnesota indicated that synthetic N was applied to corn systems at an average rate of 157 kg N ha^{-1}. Approximately 57% of the synthetic N application was applied during the spring prior to planting, while 33% was applied during the fall (Bierman et al., 2012). The average N rate from manure application was 137 kg N ha^{-1} with the majority (64%) applied during the fall (Minnesota Department of Agriculture, 2017).

In this study we used three emission inventories for comparison to the mean annual tall tower fluxes. These inventories included the National Emissions Inventory (NEI; https://www.epa.gov/air-emissions-inventories/national-emissions-inventory-nei), hemispheric transport of air pollution (HTAP_v2; http://edgar.jrc.ec.europa.eu/htap_v2), and emission database for global atmospheric research (EDGARv432; http://edgar.jrc.ec.europa.eu/overview.php?v=432_AP). NEI and HTAP make use of nationally reported emissions (i.e., provided by the Environmental Pollution Control Agency for the United States), while EDGAR uses statistical data provided by the Food and Agriculture Organization of the United Nations. Both HTAP and EDGAR provide NH_3 emissions at monthly timescales with spatial resolution of 10 km, while NEI provides an annual estimate with spatial resolution of 4 km. NEI data are provided for 2011 and EDGAR and HTAP data represent the year 2010 (Olivier et al., 1995; Reis et al., 2009).

2.7. Concentration Footprints

The Stochastic Time-Inverted Lagrangian Transport (STILT) model (Gerbig et al., 2003; Lin et al., 2003, 2004) was used to estimate the tall tower concentration source footprint using the sample inlet (receptor) at a height of 100 m. The STILT model was forced with atmospheric drivers (e.g., planetary boundary layer (PBL) height, wind, and atmospheric stability) obtained from the Weather Research and Forecasting (WRF) model version 3.8.1 (Nehrkorn et al., 2010). We released 500 particles per hour and traced the particles backward in time for 7 days for each hour of April 2017 through September 2017. The time- and volume-integrated footprint function was quantified by summing the total amount of time each particle was in a volume element over a time step, normalized by the total amount of particles. Here, we combined the STILT analyses with the NH_3 emission inventories described above to estimate the potential influence of anthropogenic sources on the tall tower observations. As a first approximation, we assumed that NH_3 is a non-reactive scalar. The concentration footprint functions are shown in Figure S12.

2.8. Statistical Analyses

All data analyses and statistical estimates were performed using MATLAB (MATLAB R2013b, The Mathworks Inc., Natick, MA, USA). The annual hourly statistical distributions of the NH_3 mixing ratios and fluxes were analyzed using a distribution fitting toolbox and chi-square test of statistical significance to provide a robust estimate of the means and standard deviations.

3. Results and Discussion

3.1. Wet Nitrogen Deposition

Weekly wet N deposition at the tall tower site typically ranged from 0 to 2.25 kg N ha^{-1} over the period DOY 260, 2016 to DOY 330, 2018 (Figure 1). The annual cumulative wet N deposition was remarkably similar for 2017 (8.8 kg N ha^{-1}, 6.1 kg NH_3-N ha^{-1}) and 2018 (8.7 kg N ha^{-1} and 5.8 kg NH_3-N ha^{-1}). These values were considerably larger (300%) than background NADP forest sites (i.e., site MN16, National Atmospheric Deposition Program, http://nadp.slh.wisc.edu/NTN/, see Figure S10). The wet N deposition values for the tall tower site were similar to NADP sites proximal to agricultural lands such as MN27 (6.4 kg N ha^{-1}), WI35 (6.3 kg N ha^{-1}), IA08 (10.1 kg N ha^{-1}) and reflect a regional NH_3 "hot spot" located within the Upper Midwest United States (i.e., Southern Minnesota, Eastern South Dakota, Southern Iowa, Northeastern Nebraska, and Western Wisconsin).

A significant period of enhanced wet N deposition occurred during the springs of 2017 and 2018 (DOY 100 to DOY 200) that coincided with the timing of intensive N fertilization application within the region. This relatively high amount of N deposition and the NH_3 concentrations observed in precipitation correlated well with elevated tall tower NH_3 mixing ratios, especially during spring and fall (Figures 1 and 2).

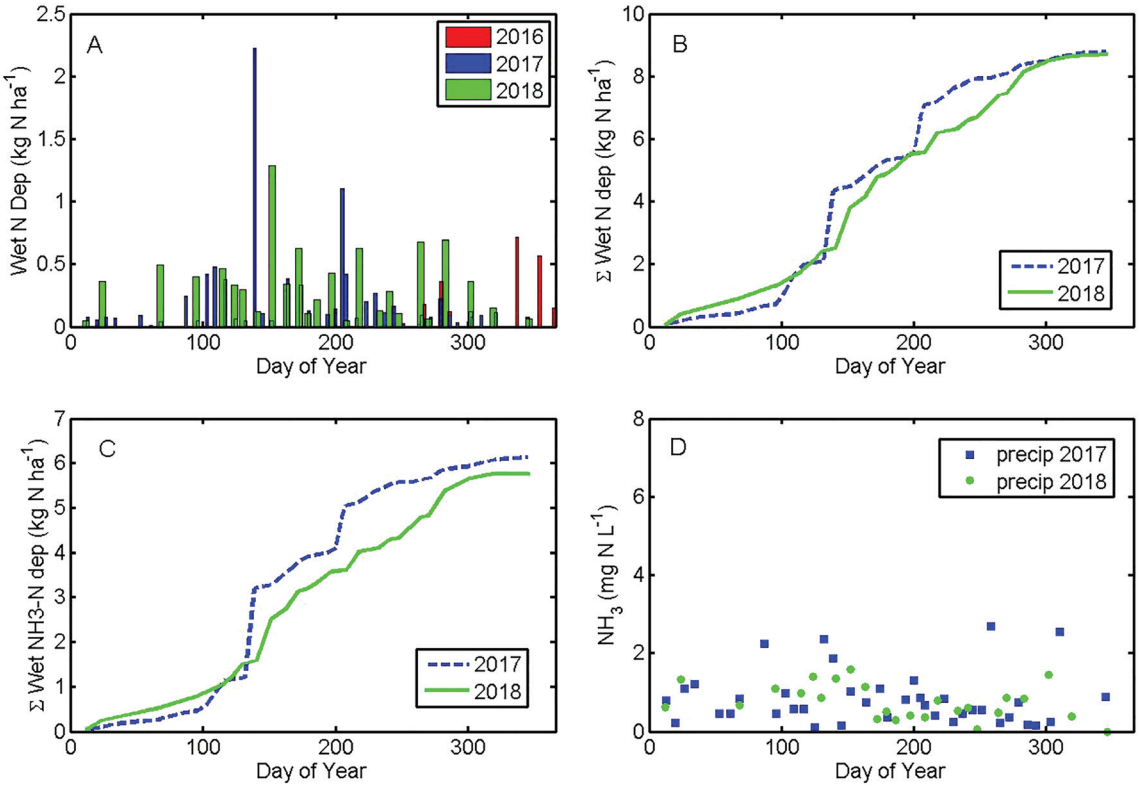


Figure 1. Wet deposition of ammonium and nitrate observed at the tall tower trace gas observatory. (a) Weekly wet N deposition; (b) cumulative wet N deposition; (c) cumulative wet ammonium deposition; and (d) ammonium concentration observed in weekly precipitation events.

3.2. Ammonia Mixing Ratios

Ammonia mixing ratios showed strong variability ranging from near zero to about 40 nmol mol^{-1} over the 21-month time series (Figure 2). This range, however, was substantially lower than that reported (i.e., 0 to 192 nmol mol^{-1}) for the 28-day tall tower campaign in Colorado USA, which is influenced by large feedlots located within 50 km (Tevlin et al., 2017). The NH_3 mixing ratios followed a Weibull statistical distribution (Figure S13) with 90% of the data within 0.10 and 18.7 nmol mol^{-1}.

Mixing ratios were highly variable, with enhancement periods likely related to agricultural activities and climate. A peak episode of elevated mixing ratios near midday on DOY 136 (May 16) of 2017 coincided with widespread N fertilizer application within the region and southerly air flow (i.e., persistent winds from approximately 160°). Ammonia mixing ratios were relatively low (median = 2.8 nmol mol^{-1}; interquartile range = 1.9 nmol mol^{-1}) from about DOY 210 to DOY 240 (July 29 to August 28, 2017) and began to increase again DOY 250 to DOY 330 (7 September to 26 November 2017) likely due to the fall application of synthetic N fertilizer and manure within the region. A large sustained enhancement in NH_3 mixing ratios was observed between DOY 320 to 330 (16 November to 26 November 2017) and was attributed to the fall application of manure and anhydrous ammonia followed by unseasonably warm air temperatures (+2.3 °C warmer than the 30-year climate normal for this period) and relatively low planetary boundary layer height (i.e., a mean ensemble diel PBL height of less than 500 m). These elevated NH_3 mixing ratios were coincident with complaints of poor air quality reported for the Saint Paul-Minneapolis metro (http://www.startribune.com/here-s-the-poop-on-monday-s-stinky-air/459095093/). Further, the precipitation data showed very high values of NH_3 concentrations for this period (Figure 1).

Ammonia mixing ratios were elevated from DOY 106 to DOY 150, 2018 and reached maximum values of about 40 nmol mol^{-1} on DOY 124 (4 May 2018). Interestingly, the NH_3 mixing ratios were considerably higher in 2018 compared to 2017. For the period 1 April to 31 August NH_3 mixing ratios were (median and interquartile range) 3.10 (3.53) and 6.98 (7.94) nmol mol^{-1}, respectively. Potential reasons for this finding are discussed in the following paragraphs and in section 3.3.

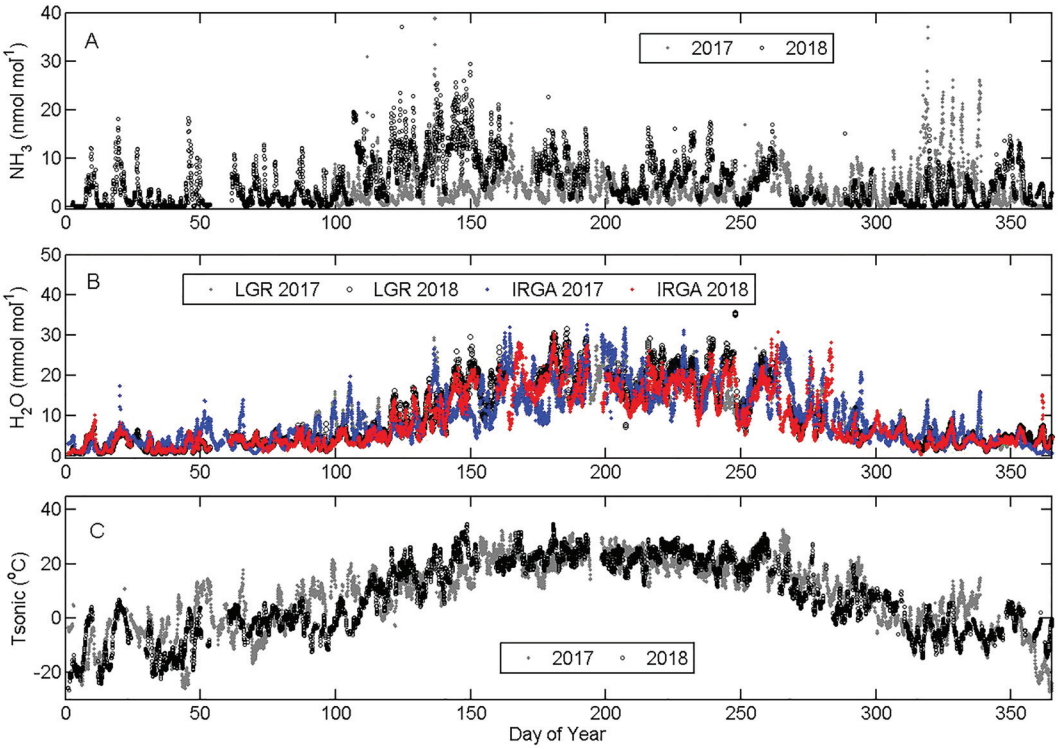


Figure 2. (a) Hourly variations of ammonia mixing ratios; (b) water vapor mixing ratios; and (c) air temperature observed at the tall tower trace gas observatory 100-m sample level over the period April 2017 to December 2018. IRGA, infrared gas analyzer; LGR, Los Gatos Research.

The tall tower NH_3 observations were compared with four AMoN sites (Figure 3) after applying a 14-day running mean filter to the tall tower observations to match the sampling resolution of the AMoN network. Overall, there is qualitative agreement in the seasonal patterns with distinct peaks observed at all sites around DOY 140 (20 May) and DOY 160 (9 June) in 2017. The strongest correlations were found between the tall tower and WI35 ($r = +0.62$) and IL37 ($r = +0.41$) sites, which are located northeast and southeast of the tall tower, respectively. The tall tower data capture the short-term dynamic nature of the NH_3 mixing ratios that cannot be detected using observations that integrate over a 2-week period. When compared to these same AMoN sites over the period 2012 to 2017, we see that the tall tower observations are consistent with the broader regional patterns of weekly and interannual variability. Further, the seasonal pattern of the tall tower NH_3 mixing ratios is in good agreement with the Atmospheric Infrared Sounder (aboard the Aqua satellite) observations (Figure 4), which show elevated mixing ratios for April to June, followed by a secondary peak in November (Warner et al., 2017). Note that for this comparison we have extracted the satellite NH_3 data from Figure 2 of Warner et al. (2017). These satellite data are representative of the Midwest United States, and the retrievals have been selected for the peak sensitivity occurring at 918 hPa.

Wind direction (source region) had a significant influence on NH_3 mixing ratios (Figure 5). For the southerly wind sector (110° to 230°), NH_3 mixing ratios showed a pronounced enhancement of up to 2 nmol mol^{-1} above the ensemble mean mixing ratio of all observations. A similar pattern has been observed for N_2O (Griffis et al., 2013). This results from the predominantly agricultural landscape to the south and major feedlot facilities located near the Minnesota-Iowa border. Our STILT footprint analyses for April to September 2017 (Figure S12) revealed that the anthropogenic NH_3 emissions were dominated by agricultural sources. For example, in April, May, June, July, August, and September, the concentration footprints indicated that 90.1%, 81.9%, 90.3%, 93.6%, 95.8%, and 92.1% of the emissions were attributed to agricultural sources within the tall tower concentration footprint.

There was a clear diel pattern and vertical gradient of NH_3 mixing ratios (Figure 5c) that varied seasonally (Figure 6). A minimum in NH_3 mixing ratios was observed from January to February. This is consistent

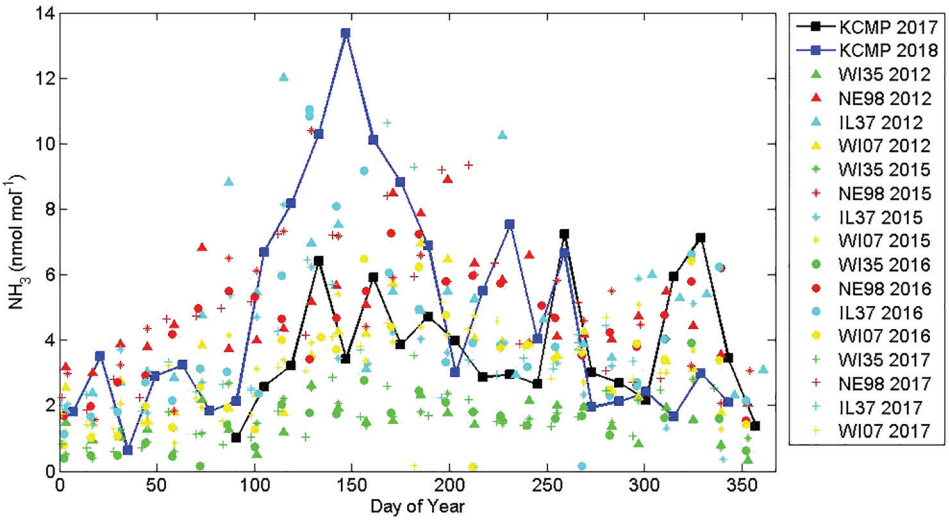


Figure 3. Comparison of ammonia mixing ratios measured at regional AMoN sites and the tall tower trace gas observatory. The tall tower hourly data have been smoothed using a 2-week running mean filter for comparison with the AMoN data. Data are shown for the tall tower (KCMP in 2017 and 2018), Wisconsin (WI35 and WI07 in 2012, 2015, 2016, and 2017), Nebraska (NE98 in 2012, 2015, 2016, 2017), and Illinois (IL37 in 2012, 2015, 2016, and 2017).

with observations from AMoN sites within the region. The highest diel amplitudes (peak to trough) were observed in the period March to April (2.2 nmol mol^{-1}) and May to June (1.8 nmol mol^{-1}). Relatively large NH_3 mixing ratios and diel amplitudes were also observed in November to December during the fall application of N fertilizers (described above). Here, strong emission strength and relatively lower planetary boundary layer heights in spring and fall contributed to the greater amplitude.

Overall, the mean ensemble NH_3 mixing ratios at the 56-m level were typically higher than at the 100-m level (Figure 5), indicating that the landscape was predominantly a net NH_3 source. The mean NH_3 mixing ratios

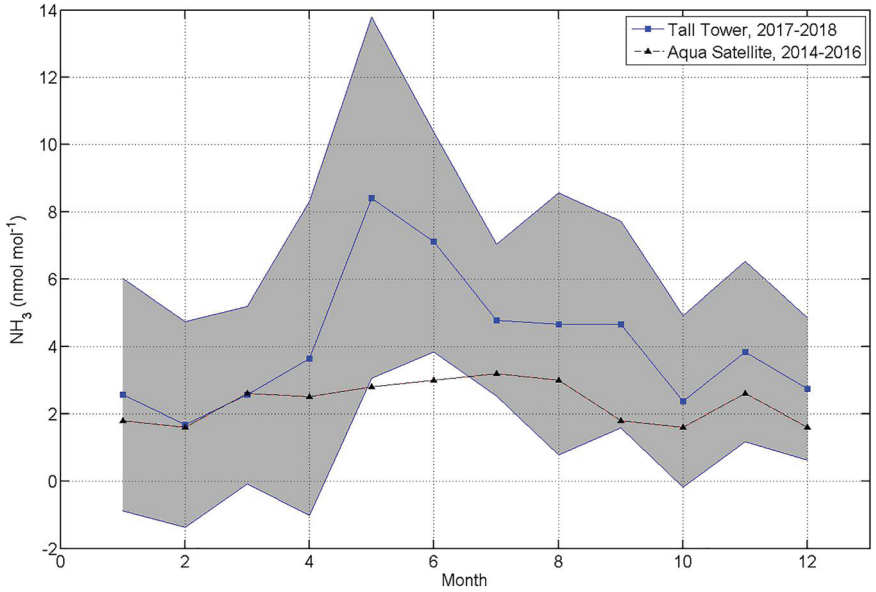


Figure 4. Comparison of ammonia mixing ratios observed by the Aqua satellite and at the tall tower trace gas observatory. The data shown represent the mean monthly values with grey shading indicating the standard error about the mean for the tall tower observations. Note that the Aqua satellite observations have peak sensitivity at approximately the 918-hPa pressure level.

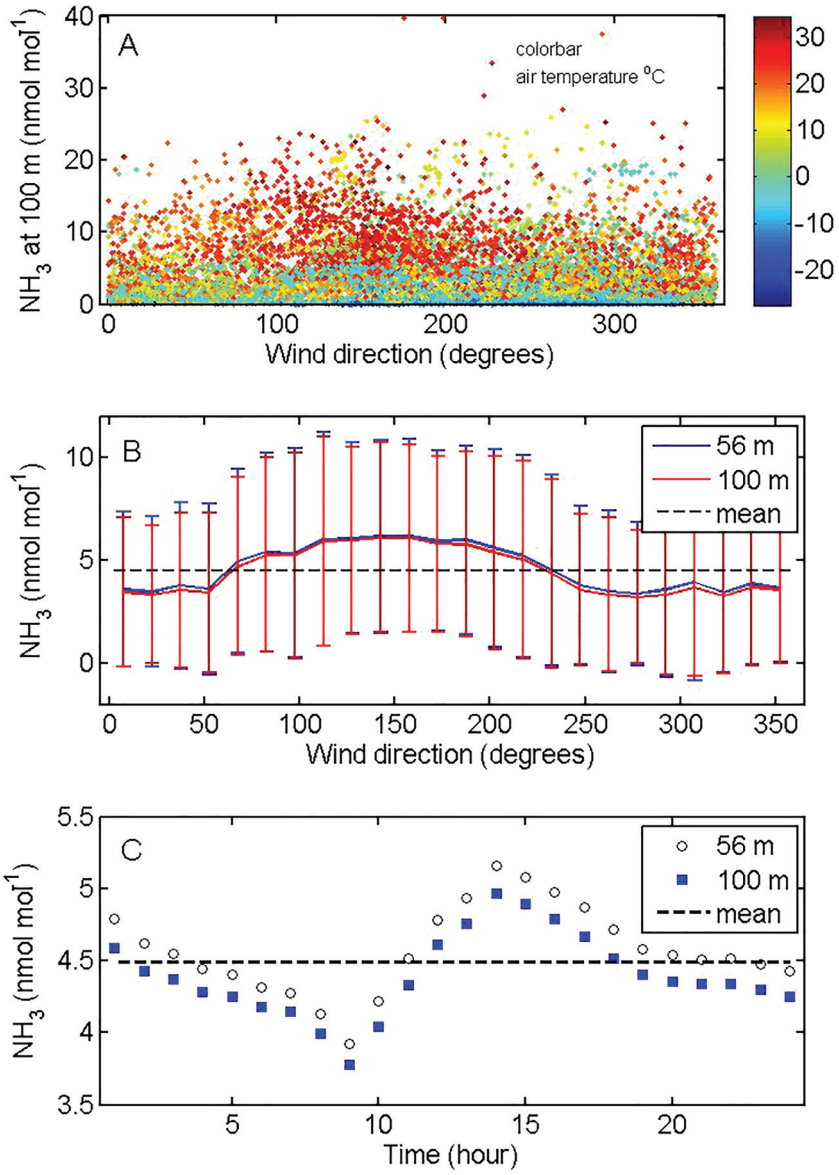


Figure 5. (a) Influence of wind direction (source area) and air temperature on ammonia mixing ratios observed at the tall tower trace gas observatory. Air temperature data are displayed using the color bar. (b) Ensemble average showing influence of wind direction on ammonia mixing ratios at the 100- and 56-m level. The horizontal dashed line indicates the mean value computed from all valid observations. (c) The ensemble dial pattern of ammonia mixing ratios observed for the 100- and 56-m levels.

for the 56- and 100-m inlets were 4.6 ± 4.6 and 4.4 ± 4.3 nmol mol^{-1}, respectively for the entire data set. Over the period April to July, the vertical NH_3 gradient was greater in 2018 (0.007 nmol mol^{-1} m^{-1}) compared to 2017 (0.003 nmol mol^{-1} m^{-1}) by a factor of 2.3. This provides further support that the higher NH_3 mixing ratios in 2018 were driven by increased NH_3 emissions. Vertical concentration gradients from the Boulder Atmospheric Observatory also revealed that NH_3 mixing ratios generally decreased away from the surface on average by about 2.7 nmol mol^{-1} (0.01 nmol mol^{-1} m^{-1}) between 10 and 280 m (Tevlin et al., 2017).

Ammonia mixing ratios are expected to be positively correlated with air temperature due to its combined effect on raising the NH_3 vapor pressure, reducing its water solubility, and enhancing the emission potential and source strength (Eilerman et al., 2016; Grant et al., 2016; Harper, 2005; Zhang et al., 2010). Further, the gas-particle phase partitioning of NH_4NO_3 is temperature dependent, where warmer air temperatures favor

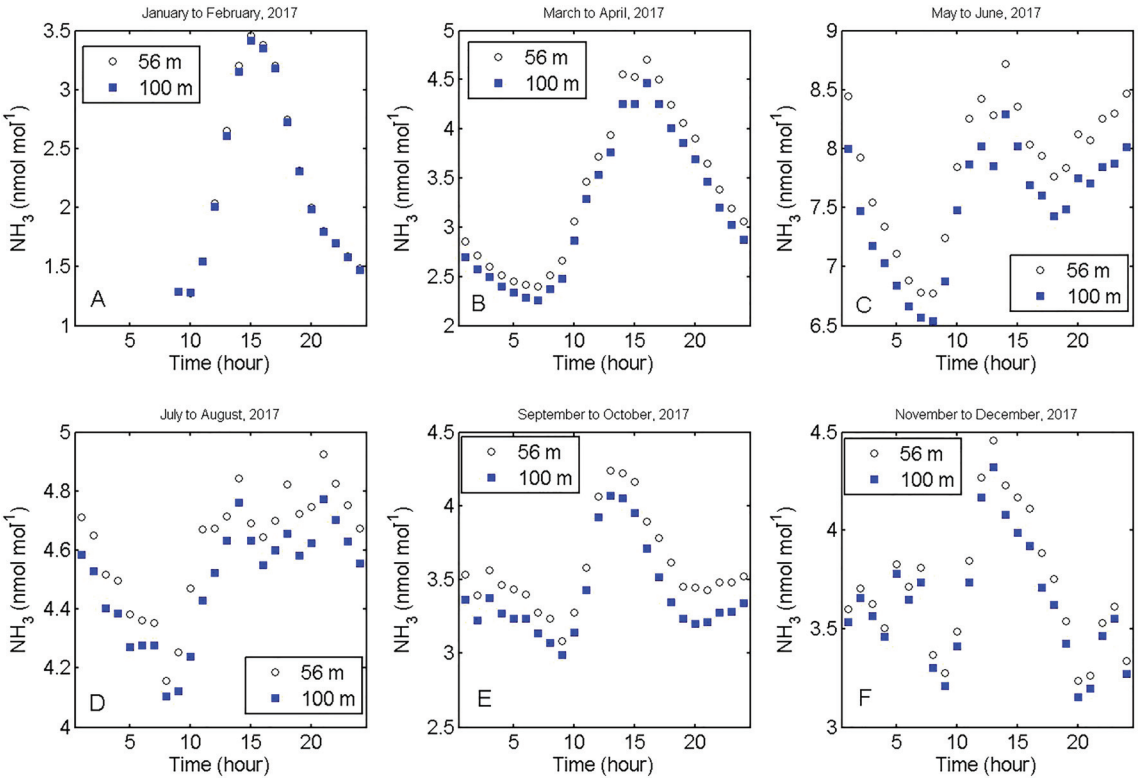


Figure 6. Monthly ensemble dial patterns of ammonia mixing ratios measured at the tall tower trace gas observatory sample inlets of 100 and 56 m.

the gas phase (Seinfeld & Pandis, 2006). Figure 7 illustrates that the sensitivity of NH_3 to air temperature was relatively consistent for different source regions (i.e., wind direction) and time periods. The sensitivity of NH_3 mixing ratios to air temperature yielded a Q_{10} of 1.44 (southerly flow) and 1.48 (northerly flow). We note that this temperature-relation is complicated by the fact that peak air temperatures typically occur during July and August when crop canopies are mature and, therefore, more likely to adsorb soil-emitted NH_3. Further, we have not directly measured the contribution of NH_4NO_3 gas-particle partitioning to ambient NH_3 mixing ratios. However, our ongoing modeling work utilizing the Weather Research and Forecasting Chemistry (WRF-CHEM) model, the low predicted particulate NH_4^+ and NO_3^- abundance (i.e., corresponding to less than 0.20 and 0.15 nmol mol^{-1}, respectively) for the study domain suggests that it plays a relatively minor role. This is further supported by local NH_4NO_3 observations from Winona, Minnesota (https://aqs.epa.gov/api), which reveal relatively low concentrations (typically <0.1 nmol mol^{-1}) during the warm season (April to September, 2017). Similar findings were reported for the Boulder Atmospheric Observatory (Tevlin et al., 2017). A review of the literature indicates that Q_{10} values typically range from about 1 to 4 for NH_3 emissions (Sutton et al., 2013; Zhang et al., 2017). Thus, the higher air temperatures observed at the tall tower during the period April to July 2018 compared to 2017 (i.e., a mean difference of +1.6 °C) also helps to explain the higher NH_3 mixing ratios and emissions observed for the same period in 2018.

3.3. Net Ecosystem NH_3 Exchange

The net ecosystem NH_3 exchange represents the bidirectional balance of emission (positive) and deposition (negative) fluxes. The hourly net ecosystem NH_3 exchange in 2017 (Figure 8) ranged from −57.4 to +65.3 nmol m^{-2} s^{-1} and exhibited a skewed Laplace distribution (Figure S14 and S15) with a mean (±1 SD) annual flux of +0.45 ± 0.97 nmol m^{-2} s^{-1}. Here, we examined the statistical distributions separately for positive (net emissions) and negative (net deposition) fluxes in order to provide a best estimate of gross emissions to the atmosphere. The unidirectional negative fluxes and positive fluxes followed a Weibull distribution (Figures S16 and S17) with a mean net deposition rate of −0.68 nmol m^{-2} s^{-1}. The mean of all

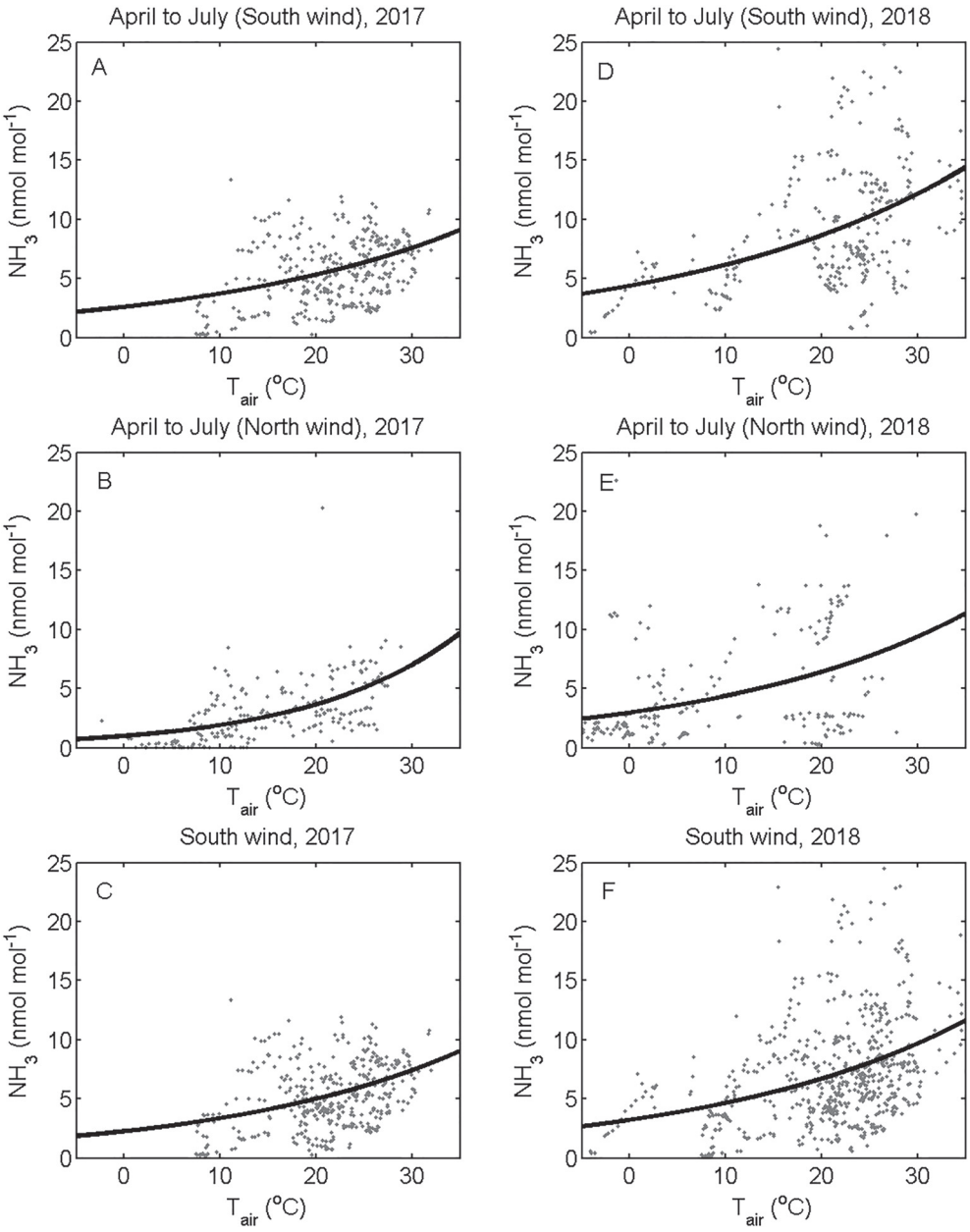


Figure 7. Sensitivity of ammonia mixing ratios to air temperature for different wind directions and time periods. A) April to July 2017 (south wind); B April to July 2017 (north wind); C South wind 2017; D. April to July 2018 (south wind); E. April to July 2018 (north wind); F. South wind 2018. Data shown are for the tall tower trace gas observatory 100-m sample level.

positive flux values was +1.24 nmol m^{-2} s^{-1}. The largest positive fluxes occurred near midday during the early growing season (May and June), following fertilization and prior to significant crop growth. Similar flux values and distributions were observed in 2018, when the mean NEE was +0.20 ± 0.77 nmol m^{-2} s^{-1} and ranged from −66.98 to +56.48 nmol m^{-2} s^{-1}. The mean of all positive and negative NEE values was +1.43 and −0.76 nmol m^{-2} s^{-1}, respectively. We note that the lower mean value for NEE in 2018 was a consequence of a more complete time series that included more wintertime (January through March) observations compared to 2017.

The ensemble diel pattern of NEE over the April to August period in 2017 and 2018 indicated peak emissions of about +0.68 and + 1.2 nmol m^{-2} s^{-1}, respectively, near midday (Figure 8). In 2017, median NEE was highest in June at midday (+1.9 nmol m^{-2} s^{-1}). Fluxes were also relatively large in November 2017 with peak late

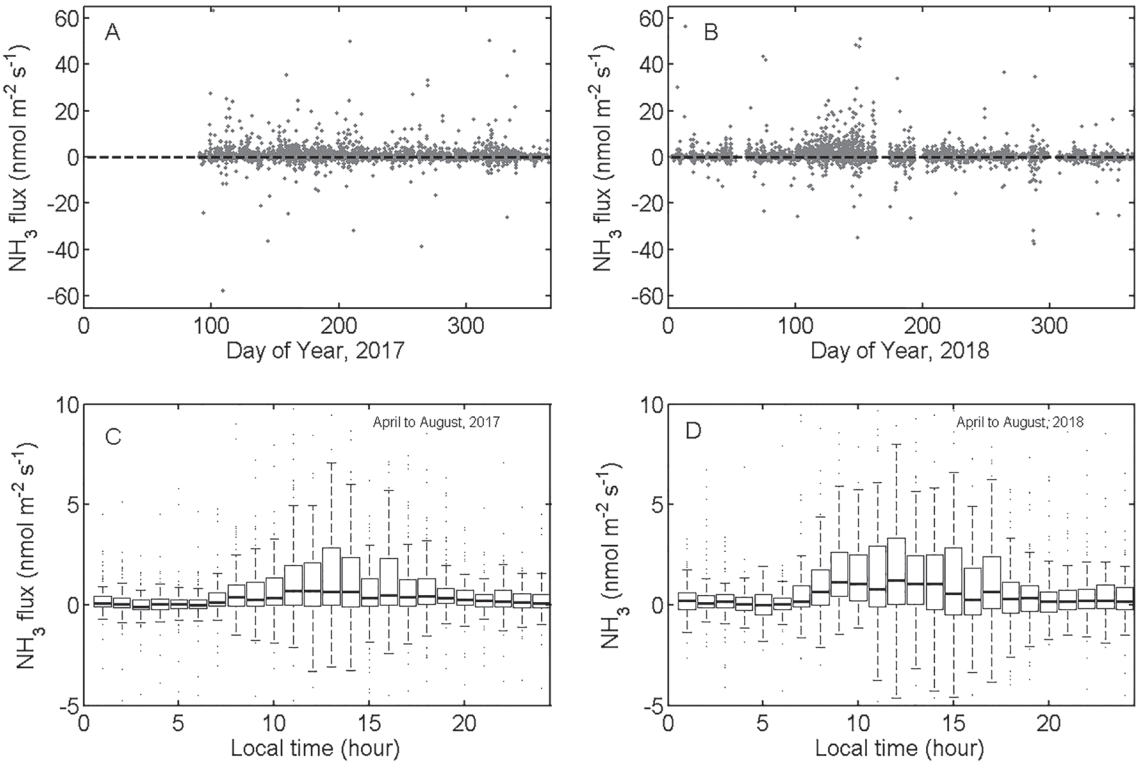


Figure 8. Hourly net ecosystem ammonia exchange measured in 2017 (a) and 2018 (b) at the tall tower trace gas observatory. Diel patterns of net ecosystem ammonia exchange are displayed as box plots for 2017 (c) and 2018 (d).

morning values of +0.80 nmol m^{-2} s^{-1}. These late season emissions likely resulted from the application of fall manure and anhydrous ammonia in combination with unseasonably warm air temperatures. Similar NEE patterns were observed in 2018. However, overall emissions were larger and median midday NEE values peaked in May 2018 at +4.1 nmol m^{-2} s^{-1}. This may be partially explained by the warmer air temperatures and increased frequency of southerly air flow during the April to August period of 2018.

Our observed fluxes are considerably lower compared to values reported for specific agricultural ecosystems, presumably because the tall tower source footprint contains approximately 54% non-agricultural lands (Zhang et al., 2014). For instance, NH_3 fluxes above a corn canopy in North Carolina during spring (DOY 149 to DOY 180) and summer (DOY 181 to DOY 213) reached mean maximum values of 47 and 6 nmol m^{-2} s^{-1}, respectively, with peak emissions occurring from late morning to midday (Walker et al., 2013). Relaxed eddy accumulation and flux-gradient NH_3 measurements above a corn canopy in the U.S. Corn Belt revealed mean fluxes of about 12 nmol m^{-2} s^{-1} with peak emissions of about 60 nmol m^{-2} s^{-1} (Nelson et al., 2019). Ammonia emissions from feedlots within the footprint of the tall tower could also be substantial. For instance, recent estimates of mean summertime emissions from beef feedlot facilities in Colorado, USA were on the order of 3 to 4 nmol m^{-2} s^{-1} with mean maximum values reaching 8 nmol m^{-2} s^{-1} (Shonkwiler & Ham, 2018).

The partitioning of NEE into its soil versus canopy fluxes indicates that crop canopies can act as a major sink for soil-emitted NH_3 (Nemitz et al., 2001; Walker et al., 2013). Past studies for example, have shown that about 70% of the soil-emitted NH_3 was taken up by a mature corn canopy (Walker et al., 2013). Here, we lacked the observations to robustly assess the partitioning of NEE at the regional scale. However, if we make use of the negative flux observations as an approximation of net dry deposition (i.e., a minimum lower bound), this suggests that mean gross emissions (i.e., approximated as NEE minus the net dry deposition) of NH_3 in 2017 and 2018 were on the order of +1.9 and +2.2 nmol m^{-2} s^{-1}, respectively. This indicates that regional canopy deposition accounted for about 30 to 40% of the gross emissions. Further, we have estimated dry NH_3 deposition based on our WRF-CHEM simulations for our study domain. These results suggest that

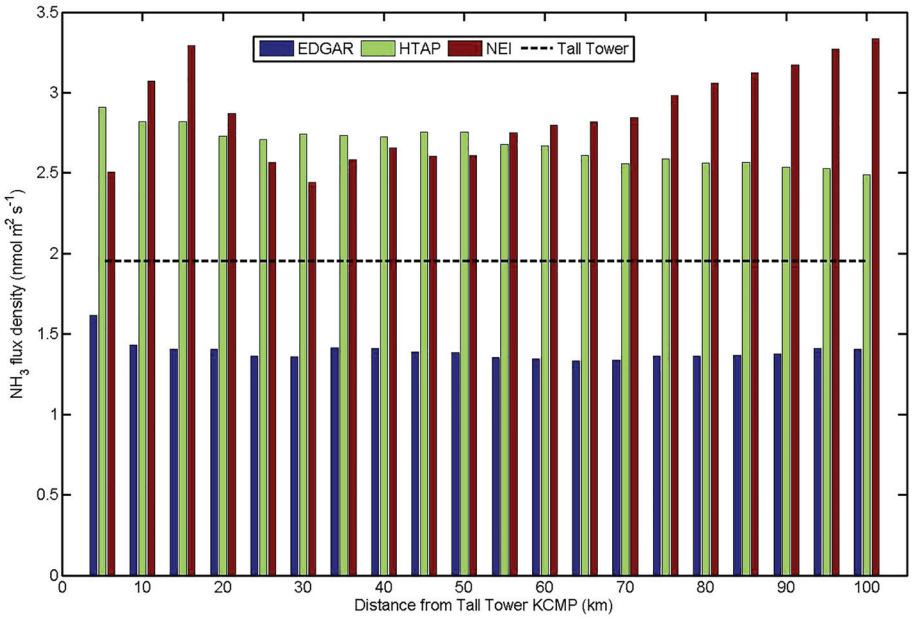


Figure 9. Average ammonia flux densities derived from emission inventories as a function of distance from the tall tower trace gas observatory. The ammonia mean flux density is also shown for the tall tower as a horizontal dashed line. EDGAR, emission database for global atmospheric research; HTAP, hemispheric transport of air pollution; NEI, national emissions inventory.

dry NH_3 deposition typically accounted for about 42% of gross NH_3 emissions for the region, which is in relative good agreement with our tall tower observations.

3.4. The Local to Regional Scale Ammonia Budget

Gross annual emissions estimated from the tall tower (+1.9 to +2.2 nmol m^{-2} s^{-1}) were greater than the mean emission inventory estimated from EDGARv431 (1.39 ± 0.06 nmol m^{-2} s^{-1}) and lower than that estimated from HTAP (2.67 ± 0.11 nmol m^{-2} s^{-1}), and NEI (2.87 ± 0.28 nmol m^{-2} s^{-1}) for a grid point containing the tall tower. These differences were relatively consistent when evaluated across spatial scales (i.e., when increasing the study domain radius from 5 to 100 km relative to the KCMP tall tower location; Figure 9). The land use characteristics of the tall tower flux footprint (i.e., within about 10 km of the tower) is approximately 43% agricultural and very similar to the tall tower concentration footprint. For example, the land use within the U.S. Corn Belt, south of the tall tower, consists of 40% agricultural land use (24% corn and 16% soybean). Overall the land use characteristics exhibit self-similarity over a broad range of distances from the tall tower through the Corn Belt (Griffis et al., 2010). This consistency in land use characteristics is also highly evident in the NH_3 emission inventory fluxes as shown in Figure 9. According to the emission inventory source partitioning, agricultural emissions were the dominant source, representing an average of 76% to 90% of the total emissions according to the spatial scale analyses of the EDGARv431 and HTAP products. When scaling up to the U.S. Corn Belt, the mean annual flux densities were 1.22 and 1.53 nmol m^{-2} s^{-1} for EDGARv431 and HTAP, respectively. Here, HTAP showed the best agreement with the tall tower observations.

If the tall tower fluxes are representative of the Upper Midwestern United States (i.e., Minnesota, Wisconsin, Iowa, Illinois, and Indiana), the gross emissions are estimated to be +720 Gg NH_3-N y^{-1}. This estimate is approximately 44% higher than recent satellite-based estimates of 500 Gg NH_3-N y^{-1} (Van Damme et al., 2014). Further, inversion estimates based on wet NH_4 deposition observations, a priori inventories, and GEOS-Chem adjoint modeling also indicate that emissions from the Midwest and Upper Midwestern United States are about 500 Gg NH_3-N y^{-1} with peak emissions occurring in April (Paulot et al., 2014). Thus, there is increasing evidence that the above emission inventories, especially NEI, are overestimated for the Upper Midwestern, United States. Paulot et al. (2014) have shown that their estimates are in good

agreement with NEI estimates from 2008 for springtime, but that summertime a priori emissions needed to be scaled down by about 50%.

If the tall tower fluxes are representative of the broader U.S. Corn Belt, the gross emissions are estimated to be +1340 Gg NH_3-N y^{-1}. This estimate is within the range of the emission inventories considered here (i.e., 800 to 1,900 Gg NH_3-N y^{-1}). The tall tower gross NH_3 emissions are considerably larger than N_2O emission estimates, which have been shown to range from 316 to 585 Gg N_2O-N y^{-1} over the period 2010 to 2015 (Chen et al., 2016; Griffis et al., 2017). Thus, the tall tower data indicate that total losses of reactive N (i.e., NH_3 + N_2O) to the atmosphere are about 1,790 Gg N y^{-1} from the U.S. Corn Belt, representing about 23% of the current annual new N input (i.e., synthetic N + biological nitrogen fixation from legumes; Griffis et al., 2017). Our future research will use the tall tower NH_3 concentration data within an inverse analysis framework (Chen et al., 2016, 2018) to provide additional constraint on these budget estimates.

4. Conclusions

Our data and analyses indicate that 90% of the hourly NH_3 mixing ratios measured at the tall tower 100-m height were between 0.10 and 18.7 nmol mol^{-1} and showed similar seasonal patterns to AMoN and satellite-based observations. The net ecosystem NH_3 exchange was greatest in spring and fall with peak hourly emissions of about +50 nmol m^{-2} s^{-1} with mean annual gross emissions of 2.1 nmol m^{-2} s^{-1}. Annual NH_3 emissions estimated using state-of-the-art inventories were 0.6- to 1.4-fold compared to the gross mean annual tall tower flux density. Our annual gross emission estimates for the Upper Midwest and broader U.S. Corn Belt regions were +720and +1,340 Gg NH_3-N y^{-1}, respectively. Finally, considering the N_2O budget over the same region, we estimated total reactive N emissions (i.e., N_2O + NH_3) of approximately +1,790 Gg N y^{-1} from the U.S. Corn Belt, representing ~23% of the current annual new N input.

Acknowledgments
This research was partially supported by the National Science Foundation (Grant 1640337), the United States Department of Agriculture National Institute of Food and Agriculture (USDA NIFA Grant 2018-67019-27808), USDA Agricultural Research Service, and the Minnesota Supercomputing Institute for Advanced Computational Research. JDW acknowledges support from the U.S. Department of Energy, Office of Science, Office of Biological and Environmental Research Program, through Oak Ridge National Laboratory's Terrestrial Ecosystem Science Science Focus Area; ORNL is managed by UT-Battelle, LLC, for the U.S. DOE under contract DE-AC05-00OR22725. Finally, we acknowledge use of the National Atmospheric Deposition Program databases. The data presented in this manuscript are available at www.biometeorology.umn.edu/research/data-archives and ESS-DIVE (Deep Insights for Earth Science Data, https://ess-dive.lbl.gov/).

References

Asman, W. A. H., Sutton, M. A., & Schjorring, J. K. (1998). Ammonia: Emission, atmospheric transport and deposition. *The New Phytologist*, *139*, 27–48.

Baker, J. M., & Griffis, T. J. (2010). A simple, accurate, field-portable mixing ratio generator and Rayleigh distillation device. *Agricultural and Forest Meteorology*, *150*, 1607–1611.

Bash, J. O., Cooter, E. J., Dennis, R. L., Walker, J. T., & Pleim, J. E. (2013). Evaluation of a regional air-quality model with bidirectional NH_3 exchange coupled to an agroecosystem model. *Biogeosciences*, *10*(3), 1635–1645. https://doi.org/10.5194/bg-10-1635-2013.

Bash, J. O., Walker, J. T., Katul, G. G., Iones, M. R., Nemitz, E., & Robarge, W. P. (2010). Estimation of in-canony ammonia sources and sinks in a fertilized zea mays field. *Environmental Science & Technology*. https://doi.org/10.1021/es9037269

Bierman, P. M., Rosen, C. J., Venterea, R. T., & Lamb, J. A. (2012). Survey of nitrogen fertilizer use on corn in Minnesota. *Agricultural Systems*, *109*, 43–52. https://doi.org/10.1016/j.agsy.2012.02.004.

Bouwman, L., Goldewijk, K. K., Van Der Hoek, K. W., Beusen, A. H. W., Van Vuuren, D. P., Willems, J., et al. (2013). Exploring global changes in nitrogen and phosphorus cycles in agriculture induced by livestock production over the 1900–2050 period. *Proceedings of the National Academy of Sciences*, *110*(52), 20882–20887. https://doi.org/10.1073/pnas.1012878108

Britto, D. T., & Kronzucker, H. J. (2002). NH4+ toxicity in higher plants: A critical review. *Journal of Plant Physiology*, *159*(3), 567–584. https://doi.org/10.1078/0176-1617-0774

Chen, Z., Griffis, T. J., Baker, J. M., Millet, D. B., Wood, J. D., Dlugokencky, E. J., et al. (2018). Source partitioning of methane emissions and its seasonality in the U.S. Midwest. *Journal of Geophysical Research: Biogeosciences*, *123*, 646–659. https://doi.org/10.1002/2017JG004356.

Chen, Z., Griffis, T. J., Millet, D. B., Wood, J. D., Lee, X., Baker, J. M., et al. (2016). Partitioning N_2O emissions within the U.S. Corn Belt using an inverse modeling approach. *Global Biogeochemical Cycles*, *30*, 1192–1205. https://doi.org/10.1002/2015GB005313.

Ciais, P., Sabine, C., Bala, G., Bopp, L., Brovkin, V., Canadell, J., et al. (2013). Carbon and other biogeochemical cycles. In T. F. Stocker, et al. (Eds.), *Climate Change 2013 - The Physical Science Basis: Contribution of Working Group I to the Fifth Assessment Report of the Intergovernmental Panel on Climate Change*, (pp. 465–570). Cambridge, United Kingdom and New York, NY, USA: Cambridge University Press.

Eilerman, S. J., Peischl, J., Neuman, J. A., Ryerson, T. B., Aikin, K. C., Holloway, M. W., et al. (2016). Characterization of ammonia, methane, and nitrous oxide emissions from concentrated animal feeding operations in Northeastern Colorado. *Environmental Science & Technology*, *50*(20), 10,885–10,893. https://doi.org/10.1021/acs.est.6b02851

Erisman, J. W., Sutton, M. A., Galloway, J., Klimont, Z., & Winiwarter, W. (2008). How a century of ammonia synthesis changed the world. *Nature Geoscience*, *1*, 636–639.

Fangmeier, A., Hadwigerfangmeier, A., Vandereerden, L., & Jager, H. J. (1994). Effects of atmospheric ammonia on vegetation—A review. *Environmental Pollution*, *86*(1), 43–82. https://doi.org/10.1016/0269-7491(94)90008-6.

Felix, J. D., Elliott, E. M., & Gay, D. A. (2017). Spatial and temporal patterns of nitrogen isotopic composition of ammonia at U.S. ammonia monitoring network sites. *Atmospheric Environment*, *150*, 434–442. https://doi.org/10.1016/j.atmosenv.2016.11.039

Gerbig, C., Lin, J. C., Wofsy, S. C., Daube, B. C., Andrews, A. E., Stephens, B. B., et al. (2003). Toward constraining regional-scale fluxes of CO_2 with atmospheric observations over a continent: 1. Observed spatial variability from airborne platforms. *Journal of Geophysical Research*, *108*(D24), 4756. https://doi.org/10.1029/2002JD003018

Grant, R. H., Boehm, M. T., & Heber, A. J. (2016). Ammonia emissions from anaerobic waste lagoons at pork production operations: Influence of climate. *Agricultural and Forest Meteorology*, *228–229*, 73–84. https://doi.org/10.1016/j.agrformet.2016.06.018

Griffis, T. J., Baker, J. M., Sargent, S. D., Erickson, M., Corcoran, J., Chen, M., & Billmark, K. (2010). Influence of C_4 vegetation on $^{13}CO_2$ discrimination and isoforcing in the Upper Midwest, United States. *Global Biogeochemical Cycles*, *24*, GB4006. https://doi.org/10.1029/2009GB003768

Griffis, T. J., Chen, Z., Baker, J. M., Wood, J. D., Millet, D. B., Lee, X., et al. (2017). Nitrous oxide emissions are enhanced in a warmer and wetter world. *Proceedings of the National Academy of Sciences*, *114*, 12,081–12,085. https://doi.org/10.1073/pnas.1704552114

Griffis, T. J., Lee, X., Baker, J. M., Russelle, M. P., Zhang, X., Venterea, R., & Millet, D. B. (2013). Reconciling the differences between top-down and bottom-up estimates of nitrous oxide emissions for the U.S. Corn Belt. *Global Biogeochemical Cycles*, *27*, 746–754. https://doi.org/10.1002/gbc.20066.

Griffis, T. J., Sargent, S. D., Baker, J. M., Lee, X., Tanner, B. D., Greene, J., et al. (2008). Direct measurement of biosphere-atmosphere isotopic CO_2 exchange using the eddy covariance technique. *Journal of Geophysical Research*, *113*, D08304. https://doi.org/10.1029/2007JD009297

Griffis, T. J., Wood, J. D., Baker, J. M., Lee, X., Xiao, K., Chen, Z., et al. (2016). Investigating the source, transport, and isotope composition of water vapor in the planetary boundary layer. *Atmospheric Chemistry and Physics*, *16*(8), 5139–5157. https://doi.org/10.5194/acp-16-5139-2016.

Harper, L. A. (2005). Ammonia: Measurement issues. In M. K. Viney, J. L. Hatfield, & J. M. Baker (Eds.), *Micrometeorology in Agricultural Systems*, *Agronomy, Monography no. 47*, (pp. 345–379). Madison, WI, USA, Madison: American Society of Agronomy.

Hicks, B.B., & Wesely, M.L., (1978). An examination of some micro-meteorological methods for measuring dry deposition. U.S.EPA Report, EPA-600/7–78-116. Research Triangle Park, North Carolina.

Krupa, S. V. (2002). Sampling and physico-chemical analysis of precipitation: A review. *Environmental Pollution*, *120*(3), 565–594.

Lin, J. C., Gerbig, C., Wofsy, S. C., Andrews, A. E., Daube, B. C., Davis, K. J., & Grainger, C. A. (2003). A near-field tool for simulating the upstream influence of atmospheric observations: The Stochastic Time-Inverted Lagrangian Transport (STILT) model. *Journal of Geophysical Research*, *108*(D16), 4493. https://doi.org/10.1029/2002JD003161

Lin, J. C., Gerbig, C., Wofsy, S. C., Andrews, A. E., Daube, B. C., Grainger, C. A., & Hollinger, D. Y. (2004). Measuring fluxes of trace gases at regional scales by Lagrangian observations: Application to the CO2 Budget and Rectification Airborne (COBRA) study. *Journal of Geophysical Research*, *109*, D15304. https://doi.org/10.1029/2004JD004754

Loubet, B., Cellier, P., Milford, C., & Sutton, M. A. (2006). A coupled dispersion and exchange model for short-range dry deposition of atmospheric ammonia. *Quarterly Journal of the Royal Meteorological Society*, *132*, 1733–1763.

Martin, N. A., Ferracci, V., Cassidy, N., & Hoffnagle, J. A. (2016). The application of a cavity ring-down spectrometer to measurements of ambient ammonia using traceable primary standard gas mixtures. *Applied Physics B: Lasers and Optics*. https://doi.org/10.1007/s00340-016-6486-9

Minnesota Department of Agriculture, (2017). Commercial nitrogen and manure fertilizer selection and management practices associated with Minnesota's 2014 corn crop, Minnesota, USA, www.mda.state.mn.us.

Minnesota Pollution Control Agency (2015). https://www.pca.state.mn.us/data/spatial-data. Web 462 site last accessed on March 1, 2019.

Nehrkorn, T., Eluszkiewicz, J., Wofsy, S. C., Lin, J. C., Gerbig, C., Longo, M., & Freitas, S. (2010). Coupled weather research and forecasting Stochastic Time-Inverted Lagrangian Transport (WRF-STILT) model. *Meteorology and Atmospheric Physics*, *107*(1–2), 51–64. https://doi.org/10.1007/s00703-010-0068-x

Nelson, A. J., Lichiheb, N., Koloutsou-Vakakis, S., Rood, M. J., Heuer, M., Myles, L. T., et al. (2019). Ammonia flux measurements above a corn canopy using relaxed eddy accumulation and a flux gradient system. *Agricultural and Forest Meteorology*, *264*, 104–113. https://doi.org/10.1016/j.agrformet.2018.10.003

Nemitz, E., Milford, C., & Sutton, M. a. (2001). A two-layer canopy compensation point model for describing bi-directional biosphere-atmosphere exchange of ammonia. *Quarterly Journal of the Royal Meteorological Society*, *127*, 815–833. https://doi.org/10.1256/smsqj.57305

Olivier, J. G. J., Bouwman, A. F., Van Der Maas, C. W. M., & Berdowski, J. J. M. (1995). Emission database for global atmospheric research (EDGAR): Version 2.0. *Studies in Environmental Science*, *65*, 651–659.

Paulot, F., & Jacob, D. J. (2014). Hidden cost of US Agricultural exports: particulate matter from ammonia emissions. *Environmental Science & Technology*, *48*(2), 903–908. https://doi.org/10.1021/es4034793.

Paulot, F., Jacob, D. J., Pinder, R. W., Bash, J. O., Travis, K., & Henze, D. K. (2014). Ammonia emissions in the United States, european union, and China derived by high-resolution inversion of ammonium wet deposition data: Interpretation with a new agricultural emissions inventory (MASAGE_NH3). *Journal of Geophysical Research: Atmospheres*, *119*, 4343–4364. https://doi.org/10.1002/2013JD021130

Pinder, R. W., Bettez, N. D., Bonan, G. B., Greaver, T. L., Wieder, W. R., Schlesinger, W. H., & Davidson, E. A. (2013). Impacts of human alteration of the nitrogen cycle in the US on radiative forcing. *Biogeochemistry*. https://doi.org/10.1007/s10533-012-9787-z

Reis, S., Pinder, R. W., Zhang, M., Lijie, G., & Sutton, M. A. (2009). Reactive nitrogen in atmospheric emission inventories. *Atmospheric Chemistry and Physics*. https://doi.org/10.5194/acp-9-7657-2009

Schlesinger, W. H. (2009). On the fate of anthropogenic nitrogen. *Proceedings of the National Academy of Sciences*, *106*(1), 203–208. https://doi.org/10.1073/pnas.0810193105

Schrader, F., Schaap, M., Zöll, U., Kranenburg, R., & Brümmer, C. (2018). The hidden cost of using low-resolution concentration data in the estimation of NH3 dry deposition fluxes. *Scientific Reports*. https://doi.org/10.1038/s41598-017-18021-6

Schwede, D. B., Schichtel, B. A., Gay, D. A., Li, Y., Chen, X., Lehmann, C. M. B., et al. (2016). Increasing importance of deposition of reduced nitrogen in the United States. *Proceedings of the National Academy of Sciences*. https://doi.org/10.1073/pnas.1525736113

Seinfeld, J. H., & Pandis, S. N. (2006). *Atmospheric Chemistry and Physics: From Air Pollution to Climate Change*, (second ed.). New York, USA: John Wiley and Sons Inc.

Shephard, M. W., Cady-Pereira, K. E., Luo, M., Henze, D. K., Pinder, R. W., Walker, J. T., et al. (2011). TES ammonia retrieval strategy and global observations of the spatial and seasonal variability of ammonia. *Atmospheric Chemistry and Physics*, *11*(20), 10743–10763. https://doi.org/10.5194/acp-11-10743-2011

Sheppard, L. J., Leith, I. D., Mizunuma, T., Neil Cape, J., Crossley, A., Leeson, S., et al. (2011). Dry deposition of ammonia gas drives species change faster than wet deposition of ammonium ions: Evidence from a long-term field manipulation. *Global Change Biology*, *17*(12), 3589–3607. https://doi.org/10.1111/j.1365-2486.2011.02478.x.

Shonkwiler, K. B., & Ham, J. M. (2018). Ammonia emissions from a beef feedlot: Comparison of inverse modeling techniques using long-path and point measurements of fenceline NH3. *Agricultural and Forest Meteorology*, *258*, 29–42. https://doi.org/10.1016/j.agrformet.2017.10.031

Sutton, M. A., Reis, S., Riddick, S. N., Dragosits, U., Nemitz, E., Theobald, M. R., et al. (2013). Towards a climate-dependent paradigm of ammonia emission and deposition. *Philosophical Transactions of the Royal Society B: Biological Sciences*, *368*(1621), 20130166. https://doi.org/10.1098/rstb.2013.0166.

Tevlin, A. G., Li, Y., Collett, J. L., McDuffie, E. E., Fischer, E. V., & Murphy, J. G. (2017). Tall tower vertical profiles and diurnal trends of ammonia in the Colorado Front Range. *Journal of Geophysical Research: Atmospheres*, *122*, 12,468–12,487. https://doi.org/10.1002/2017JD026534

Van Damme, M., Clarisse, L., Dammers, E., Liu, X., Nowak, J. B., Clerbaux, C., et al. (2015). Towards validation of ammonia (NH_3) measurements from the IASI satellite. *Atmospheric Measurement Techniques*, *8*(3), 1575–1591. https://doi.org/10.5194/amt-8-1575-2015.

Van Damme, M., Clarisse, L., Heald, C. L., Hurtmans, D., Ngadi, Y., Clerbaux, C., et al. (2014). Global distributions, time series and error characterization of atmospheric ammonia (NH_3) from IASI satellite observations. *Atmospheric Chemistry and Physics*, *14*(6), 2905–2922. https://doi.org/10.5194/acp-14-2905-2014.

Vogt, E., Dragosits, U., Braban, C. F., Theobald, M. R., Dore, A. J., van Dijk, N., et al. (2013). Heterogeneity of atmospheric ammonia at the landscape scale and consequences for environmental impact assessment. *Environmental Pollution*, *179*, 120–131. https://doi.org/10.1016/j.envpol.2013.04.014.

Walker, J. T., Jones, M. R., Bash, J. O., Myles, L., Meyers, T., Schwede, D., et al. (2013). Processes of ammonia air-surface exchange in a fertilized Zea mays canopy. *Biogeosciences*, *10*(2), 981–988. https://doi.org/10.5194/bg-10-981-2013.

Walker, J. T., Robarge, W. P., & Austin, R. (2014). Modeling of ammonia dry deposition to a pocosin landscape downwind of a large poultry facility_rfor1. *Agriculture, Ecosystems and Environment*, *185*, 161–175. https://doi.org/10.1016/j.agee.2013.10.029.

Walker, J. T., Robarge, W. P., Wu, Y., & Meyers, T. P. (2006). Measurement of bi-directional ammonia fluxes over soybean using the modified Bowen-ratio technique. *Agricultural and Forest Meteorology*. https://doi.org/10.1016/j.agrformet.2006.03.011

Warland, J. S., Dias, G. M., & Thurtell, G. W. (2001). A tunable diode laser system for ammonia flux measurements over multiple plots. *Environmental Pollution*, *114*(2), 215–221. https://doi.org/10.1016/S0269-7491(00)00218-9

Warner, J. X., Dickerson, R. R., Wei, Z., Strow, L. L., Wang, Y., & Liang, Q. (2017). Increased atmospheric ammonia over the world's major agricultural areas detected from space. *Geophysical Research Letters*, *44*, 2875–2884. https://doi.org/10.1002/2016GL072305

Wood, J. D., Griffis, T. J., Baker, J. M., Frankenberg, C., Verma, M., & Yuen, K. (2017). Multiscale analyses of solar-induced florescence and gross primary production. *Geophysical Research Letters*, *44*, 533–541. https://doi.org/10.1002/2016GL070775

Xu, J., Lee, X., Xiao, W., Cao, C., Liu, S., Wen, X., et al. (2017). Interpreting the$^{13}C/^{12}C$ ratio of carbon dioxide in an urban airshed in the Yangtze River Delta, China. *Atmospheric Chemistry and Physics*, *17*(5), 3385–3399. https://doi.org/10.5194/acp-17-3385-2017.

Zhang, L., Wright, L. P., & Asman, W. A. H. (2010). Bi-directional air-surface exchange of atmospheric ammonia: A review of measurements and a development of a big-leaf model for applications in regional-scale air-quality models. *Journal of Geophysical Research*, *115*, D20310. https://doi.org/10.1029/2009JD013589

Zhang, X., Davidson, E. A., Mauzerall, D. L., Searchinger, T. D., Dumas, P., & Shen, Y. (2015). Managing nitrogen for sustainable development. *Nature*, *528*(7580), 51–59. https://doi.org/10.1038/nature15743

Zhang, X., Lee, X., Griffis, T. J., Baker, J. M., & Xiao, W. (2014). Estimating regional greenhouse gas fluxes: An uncertainty analysis of planetary boundary layer techniques and bottom-up inventories. *Atmospheric Chemistry and Physics*, *14*, 10,705–10,719.

Zhang, X., Wu, Y., Liu, X., Reis, S., Jin, J., Dragosits, U., et al. (2017). Ammonia emissions may be substantially underestimated in China. *Environmental Science & Technology*, *51*(21), 12,089–12,096. https://doi.org/10.1021/acs.est.7b02171